AXIAL OXYGEN DIFFUSION IN THE KROGH MODEL:

Modifications to account for myocardial oxygen tension in isolated perfused rat hearts measured by EPR oximetry

Oleg Grinberg, Boris Novozhilov, Stalina Grinberg, Bruce Friedman, and Harold M. Swartz

Abstract: The cylindrical steady-state model developed by Krogh with Erlang has served as the basis of understanding oxygen supply in living tissue for over eighty years. Due to its simplicity and agreement with some observations, it has been extensively used and successfully extended to new fields, especially for situations such as drug diffusion, water transport, and ice formation in tissues. However, the applicability of the model to make even a qualitative prediction of the oxygen level of specific volumes of the tissue is still controversial. We recently have developed an approximate analytical solution of a steady-state diffusion equation for a Krogh cylinder, including oxygen concentration in the capillary. This model was used to explain our previous experimental data on myocardial pO_2 in isolated perfused rat hearts measured by EPR oximetry. An acceptable agreement with the experimental data was obtained by assuming that a known limitation of the existing EPR methods—a tendency to over-weight low pO_2 values—had resulted in an under-estimate of the pO_2. These results are consistent with recent results of others, which stress the importance of taking into account the details of what is measured by various methods.

1. INTRODUCTION

The cylindrical steady-state model developed by Krogh with Erlang has served as the basis of understanding oxygen supply in living tissue for over eighty years. The use of a

circulation unit with one axial capillary permitted a description of the oxygen transport in tissue using simple analytical functions. The simplicity of the Krogh-Erlang model, which was achieved by ignoring axial oxygen diffusion of oxygen and blood as an oxygen carrier, still attracts researchers even though more complex and potentially more accurate extensions of the concepts have been developed. These include more sophisticated mathematical models for oxygen transport in tissue (see reviews by Popel[1] and Hellums et al.[2]), studies that take into account the vascular structure,[3] and considerations of regulation of oxygen delivery.[4, 5]

1.1. Incorporation of Axial Oxygen Diffusion

One of the earliest and still widely used approaches is the Kety assumption[6] that assumes a linear decrease of oxygen concentration in the capillary from the arterial to the venous end. Several groups have now calculated the effect of axial oxygen diffusion along the capillary by solving the diffusion equation using digital methods. Fletcher and Schubert[7] have developed a model that takes into account axial diffusion and wall permeability effects in perfused capillary-tissue structures. The venous boundary conditions and the characteristic "permeability coefficient" of the vessel wall were incorporated into the model. Lagerlund and Low[8] included axial diffusion in blood and in surrounding tissue. In this simulation, it was assumed that the oxygen consumption of nerve tissue obeys Michaelis-Menten kinetics rather than zero-order kinetics, as had been assumed in the Krogh model. Analytical solutions for the radially averaged, axially distributed modified Krogh model were developed by Schubert and Zhang.[9] In this model they averaged the tissue oxygen radially, using a mass-transfer coefficient to maintain radial transport, and adding axial diffusion in the capillary and tissue.

1.2. Applications to Processes Where Hemoglobin is Not Involved in Oxygen Diffusion

Using numerical methods and an advanced Krogh model, Gabet[10] simulated injection of a drug into a capillary and its diffusion in tissues, and obtained results that were close to the experimental data. Millard and Gorman[11] used a similar approach to describe substrate concentration in tissue. Using the Krogh approach, Rubinsky and Pegg[12] developed a mathematical-model for the freezing process in biological tissue. Bischof et al.[13]; Devireddy and Bischof[14] and Devireddy et al.[15] have used the Krogh cylinder model to simulate water transport and ice formation in both isolated hepatocytes and whole tissue slices.

These studies show that the Krogh model still has great applicability to make a qualitative prediction under different experimental circumstances. These results also demonstrate that the use of digital methods makes analysis more complex. We recently have developed an approximate analytical solution of a steady-state diffusion equation for a Krogh cylinder including oxygen concentration in the capillary. This solution was used to reanalyze our previous experimental data on myocardial pO_2 in isolated perfused rat hearts measured by EPR oximetry[16] without an oxygen carrier.

2. DIFFUSION EQUATION AND BOUNDARY CONDITIONS

We considered a diffusion equation in a Krogh cylinder using cylindrical coordinates:

$$\frac{1}{r}\frac{\partial}{\partial r}\left(r\frac{\partial U}{\partial r}\right)+\frac{\partial^2 U}{\partial z^2}-\frac{Q}{D}=0 \tag{1}$$

boundary conditions in tissue $r_0 \le r \le R$, $0 \le z \le L$:

$$z=0,\ \frac{\partial U}{\partial z}=0;\ z=L,\ \frac{\partial U}{\partial z}=0; \tag{2a}$$

$$r=R,\ \frac{\partial U}{\partial r}=0;\ r=r_0,\ U_c=U\big|_{r_0} \tag{2b}$$

and boundary conditions in the capillary $0 < r < r_0$, $0 \le z \le L$:

$$\pi r_0^2 V\frac{dU_c}{dz}=2\pi r_0 D\frac{\partial U}{\partial r}\bigg|_{r_0},\ U_c(0)=U_0 \tag{3}$$

where $U=U(r,z)$, $Uc=U(r,z)$ are oxygen concentrations in tissue and capillary, respectively, Q is zero order oxygen consumption, D is oxygen diffusion coefficient, R and L are radius and length of Krogh cylinder respectively, r_0 is radius of capillary, V is speed of media in the capillary, and U_0 is oxygen concentration in capillary at the arterial end of capillary.

To solve the problem the following dimensionless variables and parameters were introduced:

$$\varphi=\frac{U}{U_0},\ \varphi_c=\frac{U_c}{U_0},\ \xi=\frac{r}{R},\ \eta=\frac{z}{R} \tag{4a}$$

$$a=\frac{r_0}{R},\ l=\frac{L}{R} \tag{4b}$$

$$u=\frac{r_0 V}{2D},\ q=\frac{QR^2}{DU_0} \tag{4c}$$

Using these variables and parameters, one can write the dimensionless diffusion equation and boundary conditions: diffusion equation in tissue

$$a \le \xi \le 1,\ 0 \le \eta \le l$$

$$\frac{1}{\xi}\frac{\partial}{\partial \xi}\left(\xi \frac{\partial \varphi}{\partial \xi}\right) + \frac{\partial^2 \varphi}{\partial \eta^2} - q = 0 \tag{5}$$

with boundary conditions:

$$\eta = 0,\ \frac{\partial \varphi}{\partial \eta} = 0;\ \eta = l,\ \frac{\partial \varphi}{\partial \eta} = 0;\ \xi = 1,\ \frac{\partial \varphi}{\partial \xi} = 0 \tag{6}$$

and in capillary:

$$0 \le \eta \le l$$

$$u\frac{d\varphi_c}{d\eta} = \left.\frac{\partial \varphi}{\partial \xi}\right|_a \tag{7}$$

$$\eta = 0,\ \varphi_c = 1 \tag{8}$$

3. RESULTS AND DISCUSSION

3.1. The Solutions of the Diffusion Equation in a Krogh Cylinder

The solutions of the Eqs. (4)-(8) are expressed as follows:

$$\varphi = A_0 - \frac{q}{4}\left(2\ln\xi - \xi^2\right) + \sum_{n=1}^{\infty} A_n F_n(\xi)\cos\gamma_n \eta \tag{9}$$

where:

$$F_n(\xi) = K_1(\gamma_n)I_0(\gamma_n \xi) + I_1(\gamma_n)K_0(\gamma_n \xi) \tag{10a}$$

$$\gamma_n = \frac{n\pi}{l},\ n = 1,\ 2,\ \ldots \tag{10b}$$

and:

$$\varphi_c = 1 - \frac{q\left(1-a^2\right)}{2au}\eta + \frac{1}{u}\sum_{n=1}^{\infty} A_n M_n \sin\gamma_n \eta, \tag{11}$$

where:

$$M_n = K_1(\gamma_n)I_1(\gamma_n a) - I_1(\gamma_n)K_1(\gamma_n a) \tag{11a}$$

and A_n should be found from the following set of linear equations:

$$A_0 = 1 + \frac{q}{4}\left[2\ln a - a^2 - \frac{l(1-a^2)}{au}\right] + \frac{1}{\pi u}\sum_{k=1}^{\infty}\frac{1-(-1)^k}{k}A_k M_k \tag{12}$$

$$A_n F_n = \frac{1-(-1)^n}{n^2}\frac{ql(1-a^2)}{\pi^2 au} + \frac{2}{\pi u}\sum_{k=1}^{\infty}k\frac{1-(-1)^{k+n}}{k^2-n^2}A_k M_k, \quad n = 1,2.. \tag{12a}$$

3.2. Calculation Procedure and Results of Computing

Using Eqs. (9)-(12), the discrete oxygen distribution in a Krogh cylinder was digitally derived (40x40 points) using numerical values of parameters for the rat heart that were chosen based on measurements of others and our experimental data. Linear Eqs. (12)-(12a) were solved using MathCAD software. This software also was used for all other calculations. Three modes of approximation (n = 3) were used for calculations in this modeling.

The discrete oxygen distribution in the plane perpendicular to the capillary at any point z_i of the capillary can be presented using the classical Krogh formula:

$$pO_2(z_i, r_j) = pO_2^{cap}(z_i) - \frac{Q}{4\alpha D}\left(2R^2\ln\left(\frac{r_j}{r_0}\right) - (r_j^2 - r_0^2)\right) \tag{13}$$

where $pO_2^{cap}(z_i)$ is the oxygen concentration in the capillary at the point z_i, $\alpha = 1.32*10^{-9}$ moles/ml/mmHg is oxygen solubility, $D = 1*10^{-5}$ cm^2/sec is oxygen diffusion coefficient, $r_0 = 2.2$ μm is capillary radius, Q is oxygen consumption of 1 cm^3 of tissue, $R = \sqrt{1/(2\sqrt{3}D_c)}$ is radius of Krogh cylinder, $D_c = 2500$ mm^{-2} is capillary density, r_j is radial coordinate, and $r_0 \geq r_j \geq R$.

Assuming that both the oxygen consumption of the tissue throughout the length of the cylinder as well as radially, and the linear velocity of the blood through the tissue are constant, Kety came to the conclusion that the oxygen concentration of the blood must fall linearly with distance as the blood traverses the capillary from arterial to the venous end. Blood is not involved in oxygen transport in isolated rat hearts perfused with crystalloid solutions. Therefore, using the Kety assumption, the oxygen concentration in the capillary $\alpha*pO_2^{cap}(z_i)$ can be expressed as follows:

$$\alpha*pO_2^{cap}(z_i) = \alpha*pO_2^{in} - (Q*z_i)/(F*L) \tag{14}$$

where pO_2^{in} is influent oxygen, F is flow rate per 1 cm^3 of tissue, and L=0.02 cm is capillary length.

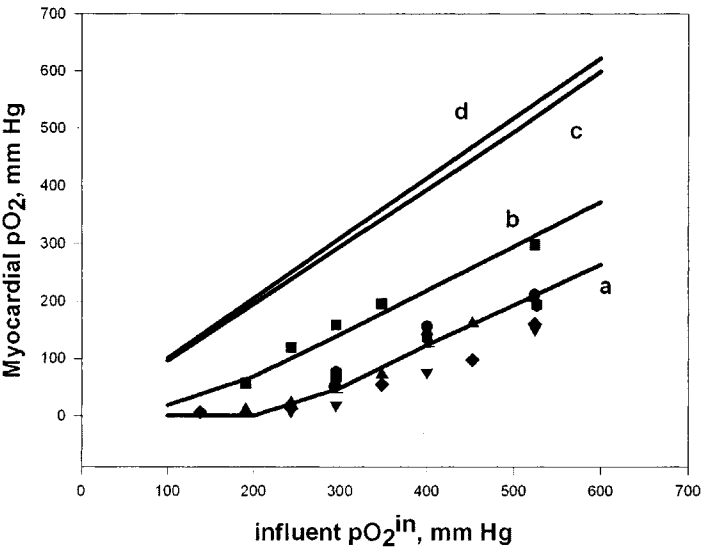

Figure 1. Modeling of myocardial pO_2 at varying influent oxygen levels using the Krogh model with (*a, b*), and without axial oxygen diffusion (*c, d*). pO_2 was derived using the LW of averaged EPR spectrum (*a, c*) and the mean pO_2 over Krogh cylinder (*b, d*). Experimental data from several different isolated hearts are represented by different symbols.[16]

We found that the oxygen distribution derived using Eqs. (9)-(12) was significantly different from the distribution given by the classical Krogh model [Eqs. (13)-(14)]. In order to compare these two models with experimental data,[16] the mean pO_2 value $<pO_2(z_i, r_j)>$ over Krogh cylinder was calculated using our analytical solution [Eqs. (9)-(12)] and the classical Krogh model with the Kety assumption [Eqs. (13)-(14)]:

$$< pO_2(z_i,r_j) >= \frac{1}{N^2} \sum_i \sum_j pO_2(z_i,r_j) \tag{15}$$

In those experiments, a constant flow experimental setup was used. When the effect of influent oxygen on myocardial pO_2 was investigated, the effect of pO_2^{in} on oxygen consumption was observed to be: [$Q=10^{-9}*(45.9+0.148*pO_2^{in})$ moles/sec/g]. In the set of experiments where the effect of flow rate (F) on myocardial pO_2 was investigated, the effects of F on influent oxygen [$pO_2^{in}=313.3+469.9*F$] and on oxygen consumption [$Q = 10^{-9}*(87.5+125*F)$ moles/sec/g] were found (flow rate was varied from 10 to 20 ml/min).

Figures 1 and 2 show the results of these calculations. One can see that the solutions with axial oxygen diffusion give a better fit to the experimental results: the mean pO_2 computed using measured oxygen consumption and flow rate is closer to the measured myocardial pO_2 in isolated perfused rat hearts. Of course, it is possible to improve the agreement with the classical Krogh model, but this requires increasing the oxygen consumption in the calculations to unexpected levels.

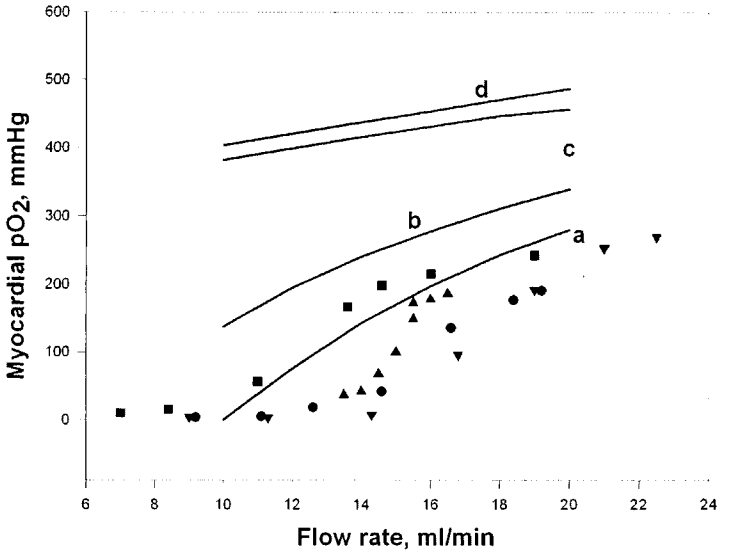

Figure 2. Modeling of myocardial pO_2 at varying flow rates using the Krogh model with (a, b) and without (d, c) axial oxygen diffusion. pO_2 was derived using the mean pO_2 over the Krogh cylinder (b, d) and LW of averaged EPR spectrum (a, c). Experimental data in isolated hearts are indicated by different symbols.

In addition, Figures 1 and 2 also show that both calculations give higher pO_2 levels than were observed experimentally. We could get a result that was consistent with expected physiology and the model by assuming that a known limitation of the existing EPR methods—a tendency to over-weight low pO_2 values—had resulted in an under-estimate of the pO_2. The pO_2 at each point of the Krogh cylinder was simulated as individual EPR lines, and the experimentally observed EPR line was computed by averaging these 40x40 spectra.

$$LW_{i,j} = a + b * pO_2(x_i, r_j) \tag{16}$$

$$RPRLine(h) = \frac{1}{N^2} \sum_i \sum_j \frac{LW_{i,j} * h}{[3*(LW_{i,j})^2 + h^2]^2} \tag{17}$$

Then pO_2(EPR) = c+d*LW is derived using the LW of the EPRline(h), where a, b, c, and d are calibration coefficients derived by calibration of LiPc crystals *in vitro* (N=40). This assumption is equivalent to the assumption that small LiPc crystals are located at each point of the Krogh cylinder. The mean pO_2 value then was calculated using this averaged spectrum and the LiPc calibration. Using this approach, an acceptable agreement with the experimental data was obtained: both the dependences of pO_2 versus flow rate and pO_2 versus influent oxygen were successfully described, Figures 1 and 2. We are developing methods of spectral analysis that will enable us to correct for the tendency to over-weight low values in a heterogeneous environment; in the future we should be able to utilize fully the improved model.

4. CONCLUSIONS

The inclusion of axial oxygen diffusion in the Krogh model and the mean pO_2 value calculated using the LW of the averaged EPR spectrum lead to better agreement between the computed and the experimental pO_2 in the isolated rat heart for these experimental conditions. These results are consistent with recent results of others that stress the importance of taking into account the details of what is measured by various methods, so that they can be compared accurately with other results and evaluated properly by models.[17]

5. ACKNOWLEDGEMENTS

This work was supported by PO1 EB002180, "Measurement of pO_2 in Tissues in Vivo and in Vitro," and used the facilities of P41 EB002032, "EPR Center for the Study of Viable Systems."

REFERENCES

1. A. S. Popel, Theory of oxygen transport to tissue, *Crit. Rev. Biomed. Eng.* **17**(3), 257-321 (1989).
2. J. D. Hellums, P. K. Nair, N. S. Hugang, and N. Ohshima, Simulation of intraluminal gas transport process in microcirculation, *Ann. Biomed. Eng.* **24**(1), 1-24 (1996).
3. M. Sharan, and A. Popel, A compartmental model for oxygen transport in brain microcirculation in the presence of blood substitutes, *J. Theor. Biol.* **216**(4), 479-500 (2002).
4. F. Hyder, R. G. Shulman, and D. L. Rothman, A model for the regulation of cerebral oxygen delivery, *J. Appl. Physiol.* **85**(2), 554-564 (1998).
5. C. A. Lodi, A. T. Minassian, L. Beydon, and M. Ursino, Modeling cerebral outoregulation and CO_2 reactivity in patients with severe head injury, *Am. J. Physiol.* **274** (5 Pt. 2), H1729-H1741 (1998).
6. S. S. Kety, Determination of tissue oxygen tension, *Fed. Proc.* **16**, 666-670 (1957).
7. J. E. Fletcher, and R.W. Schubert, Axial diffusion and wall permeability effects in perfused capillary-tissue structures, *Biosystems* **20**(2), 153-174 (1987).
8. T. D. Lagerlund, and P. A. Low, Axial diffusion and Michaelis-Menten kinetics in oxygen delivery in rat peripheral-nerve, *Am. J. Physiol.* **260** (2 Pt. 2), R430-R440 (1991).
9. R. W. Schubert, and X. Zhang, The equivalent Krogh cylinder and axial oxygen transport, Oxygen Transport to Tissue XVIII, *Adv. Exper. Med. Biol.* **411**, 191-202 (1997).
10. L. Gabet, Capillary net and injection modeling, *Int. J. BioMed. Comp.* **31**(1), 25-36 (1992).
11. C. A. Millard, and A. D. Gorman, A model for substrate concentrations in tissue surrounding single capillaries, *Math. Comp. Model.* **25**(11), 1-7 (1997).
12. B. Rubinsky, and D. E. Pegg, A mathematical-model for the freezing process in biological tissue, *Cryobiol.* **25**(6), 546 (1988).
13. J. C. Bischof, C. M. Ryan, R. G. Tompkins, M. L.Yarmush, and M. Toner, Ice formation in isolated human hepatocytes and human liver tissue, *ASAIO J.* **43**(4), 271-278 (1997).
14. R. V. Devireddy, and J. C. Bischof, Measurement of water transport during freezing in mammalian liver tissue: Part II - The use of differential scanning calorimetry, *J. Biomech. Eng. (Transactions of the ASME)* **120**(5), 559-569 (1998).
15. R. V. Devireddy, J. E. Coad, and J. C. Bischof, Microscopic and calorimetric assessment of freezing processes in uterine fibroid tumor tissue, *Cryobiol.* **42**(4), 225-243 (2001).
16. B. J. Friedman, O. Y. Grinberg, K. A. Isaacs, T. M. Walczak, and H. M. Swartz, Myocardial oxygen-tension and relative capillary density in isolated-perfused rat hearts, *J. Mol. Cell. Cardiol.* **27**(12), 2551-2558 (1995).
17. I. Tomas-Das, A. Waites, A. Das, and J. Denekamp, Theoretical simulation of oxygen tension measurement in tissues using a microelectrode: I. The response function of the electrode, *Physiol. Measur.* **22**(4),713-725 (2001).